Magnetotransport of proton-irradiated $BaFe_2As_2$ and $BaFe_{1.985}Co_{0.015}As_2$ single crystals

D. A. Moseley,[1,*] K. A. Yates,[1] N. Peng,[2] D. Mandrus,[3,4] A. S. Sefat,[4] W. R. Branford,[1] and L. F. Cohen[1,†]

[1]*Blackett Laboratory, Imperial College, London SW7 2BZ, United Kingdom*

[2]*Surrey Ion Beam Centre, ATI, Faculty of Engineering and Physical Sciences, University of Surrey, Guildford GU2 7XH, United Kingdom*

[3]*Department of Materials Science and Engineering, University of Tennessee, Knoxville, Tennessee 37996, USA*

[4]*Materials Science and Technology Division, Oak Ridge National Laboratory, Oak Ridge, Tennessee 37831, USA*

(Received 21 June 2014; revised manuscript received 5 January 2015; published 17 February 2015)

Here we study the magnetotransport properties of the ferropnictide crystals $BaFe_2As_2$ and $BaFe_{1.985}Co_{0.015}As_2$. These materials exhibit a high field linear magnetoresistance that has been attributed to the quantum linear magnetoresistance model. In this model, the linear magnetoresistance is dependent on the concentration of scattering centers in the material. By using proton-beam irradiation to change the defect scattering density, we find that the dependence of the magnitude of the linear magnetoresistance on scattering quite clearly contravenes this prediction. A number of other scaling trends in the magnetoresistance and high field Hall data are observed and discussed.

DOI: 10.1103/PhysRevB.91.054512 PACS number(s): 72.10.Fk, 74.25.F−, 74.70.Xa

The ferropnictides are a remarkable system where the competing influences of electron correlations, magnetic ordering effects, and crystal structure combine to create a range of extraordinary properties including superconductivity [1–3]. In all underdoped ferropnictides, associated structural (tetragonal to orthorhombic) and antiferromagnetic (AFM) transitions occur, which in parent $BaFe_2As_2$ are coupled at around 134 K [2,4]. At the magnetic transition [1,5], a spin-density wave (SDW) striped magnetic state is produced, with the spins aligned antiparallel along the *a*- and *c*-axis directions and parallel in the *b*-axis direction. Discrepancies between the experimental and theoretical local moment calculations [6,7] indicate that the system fits neither entirely local nor itinerant models. Simultaneous to the establishment of the AFM ordering is the creation of extremely small Fermi surface (FS) pockets [8]. It has been theoretically predicted [9] and verified by angle-resolved photoemission spectroscopy (ARPES) measurements [10] that some of these FS pockets have Dirac cone (DC) characteristics, where a linear relationship between momentum and energy is expected. DCs have been recently discovered in a wide variety of different materials, with many possessing a two-dimensional structure similar to $BaFe_2As_2$ [11], making the study of DC physics a topic of general interest in condensed-matter physics today.

Large positive linear magnetoresistance (MR) is rather rare but is often found in DC systems. Generally, in the ferropnictides this has been attributed to the Abrikosov quantum linear magnetoresistance (QLM) model [8,12–14] on the basis that the extreme quantum limit (EQL) condition of the model (all carriers occupying a single Landau level) is accessible at much lower fields in Dirac systems. However, doubts have been raised about the robustness of this phenomenon [15]. The QLM model predicts a strong dependence of the MR on the concentration of scattering centers, N_i. Two regimes have been identified; in the compensated regime the MR is inversely proportional to N_i and in the uncompensated regime the MR is linearly proportional to N_i. Thus, a systematic study of the MR as a function of N_i is a good test of the applicability of the QLM model in these systems.

Proton irradiation has been shown to introduce defects, which are recognized to be predominantly of a point defect character, without significantly altering the electronic structure of the material [16,17]. In contrast, Co doping is expected to modulate both the scattering and the carrier concentration. In this paper, we present resistivity, MR, and Hall effect measurements on pristine and proton-irradiated single crystals of $BaFe_2As_2$ and $BaFe_{1.985}Co_{0.015}As_2$ and compare our findings with the predictions of the QLM model.

The in-plane MR shows unsaturated linear magnetic field dependence in all crystals below the structural and magnetic transitions. The crossover to linear MR behavior occurs at a temperature-dependent critical field (B^*) which we find is unaffected by the proton irradiation. A number of other scaling trends in the MR and high field Hall data are observed, which are discussed in light of both the multiband and anisotropic quasiparticle lifetime models.

The paper first introduces the QLM model, then describes our experimental efforts to compare systematic changes in the scattering density to the predictions of the QLM model. Finally we discuss the high field Hall resistance data and observation of scaling relationships.

I. INTRODUCTION TO QUANTUM LINEAR MAGNETORESISTANCE

Previous work has reported a linear MR occurring at low magnetic fields in twinned crystals [8,13,14]. There are a number of potential explanations for the advent of linear MR [18–22]; however, the QLM model [23,24] has been generally applied to the ferropnictides [8,13,14]. The requirements for QLM are extremely stringent, as the carriers within the dominant bands must be confined to a single Landau level. This condition can only be satisfied at the fields utilized within this work if the dominant transport bands are extremely small DCs [8,13,14,25]. Using the separation of Landau levels within DCs it is possible to write the conditions for the EQL,

$$n_0 \ll \left(\frac{e\mu_0 H}{\hbar}\right)^{3/2} T_0 < v_f\sqrt{e\mu_0 H\hbar}, \qquad (1)$$

*dam06@ic.ac.uk
†l.cohen@ic.ac.uk

where n_0 and T_0 are the EQL threshold values for the carrier density and temperature, respectively. It has therefore been interpreted that the linear MR is evidence for the existence of DCs. In most instances, the linear MR originates at fields above 1 T. At low fields, a semiclassical parabolic shape is perceived [MR $\approx A_2(\mu_0 H)^2$]. At B^*, a transition from the low field parabolic behavior to the high field linear MR is discerned; therefore, above and below B^* we write

$$\mathrm{MR} \approx \begin{cases} A_2[\mu_0 H]^2, & \mu_0 H < B^*, \\ A_1 \mu_0 H + O[\mu_0 H]^2, & \mu_0 H > B^*. \end{cases} \quad (2)$$

Furthermore, by rearranging the temperature condition for the EQL [right-hand condition of Eq. (1)] it is possible to determine an expected temperature dependence of B^* [8],

$$B^*(T) = \frac{1}{2\hbar e v_f^2}(k_b T + E_F)^2, \quad (3)$$

from which the Fermi velocity and energy can be calculated.

There are a number of different forms of the QLM model, each dependent on the electronic structure of the material [24]. In the case of $BaFe_2As_2$ and $BaFe_{1.985}Co_{0.015}As_2$, the situation of small pockets of high-mobility carriers within a FS is most applicable. Within this scheme there are two forms for ideally compensated or uncompensated metals, where compensated specifically refers to the equal numbers of carriers within the high-mobility pockets. The simplification for the compensated case leads to

$$\rho_{xx}(\mu_0 H) = \frac{\pi \mu_0 H}{f(\mathbf{n}) e N_i}, \quad (4)$$

where $f(\mathbf{n})$ is a function with a value close to unity. However, in the uncompensated situation,

$$\rho_{xx}(\mu_0 H) = \frac{f(\mathbf{n}) N_i \mu_0 H}{e(n_e - n_h)^2} = \frac{f(\mathbf{n}) N_i \mu_0 H}{e n_{\mathrm{eff}}^2}, \quad (5)$$

where n_e and n_h are the electron and hole carrier densities, respectively, and n_{eff} is the effective carrier density within the DCs.

As illustrated by Eqs. (4) and (5), the compensated and uncompensated models have different dependencies on the scattering density, with the compensated (uncompensated) models displaying indirect (direct) proportionality. A variation of Eq. (5) has been applied throughout the literature where the difference between the electron and hole carrier densities has been replaced with the "effective" carrier density (n_{eff}) for the DC states derived from the low field Hall resistivity [8,13].

II. EXPERIMENTAL DETAILS

Large single crystals of $BaFe_2As_2$ and $BaFe_{1.985}Co_{0.015}As_2$, grown using the self-flux method [26], were cleaved using a micromechanical exfoliation technique. All crystals were cleaved from the same crystal for each compound. Proton irradiation was performed such that protons doses of 0.5×10^{16} and 1×10^{16} cm^{-2} were achieved for the $BaFe_{1.985}Co_{0.015}As_2$ crystals and 0.5×10^{16} cm^{-2} for $BaFe_2As_2$. Crystal sizes were of the order of 2 mm in the *ab* plane and below 40 μm along the *c* axis. This is sufficiently thin (<50 μm) to achieve homogeneous irradiation damage using 3-MeV H^+ irradiation for $BaFe_2As_2$ according to calculations using the SRIM code [17]. All transport measurements were taken using the van der Pauw technique [27] with the magnetic field applied along the *c* axis and current within the *ab* plane. Data were symmetrized by combining the MR responses of 0 to 7 T positive (0 to −7 T negative) magnetic sweep to the −7 to 0 T negative (7 to 0 T positive) sweep creating two continuous sets of data. The MR response for all sweep directions was then averaged to ensure the elimination of the Hall voltage signal. Two forms of the MR are presented in this work, the MR is defined as $[\rho(\mu_0 H) - \rho(0T)]$ (defined as MR throughout) and the normalized MR (NMR) as $[\frac{\rho(\mu_0 H) - \rho(0T)}{\rho(0T)}]$.

A rigorous treatment of the transport characteristics requires a multiband approach [28]; nevertheless, to examine trends between unirradiated and irradiated undoped and Co-doped crystals, we restrict our analysis to low fields and consider a single carrier approximation to extract n_{eff} from the low field Hall resistivity as

$$n_{\mathrm{eff}} = \frac{1}{R_H e}, \quad (6)$$

where R_H is the Hall coefficient. From this and the longitudinal resistivity we can also extract the effective single carrier Hall mobility μ_H.

III. RESULTS

A. Testing the QLM model

In order to test the QLM model, we first must demonstrate that we have changed the scattering density in our crystals without significantly altering other properties. Figure 1 shows the zero-field resistivity (ρ_0) vs T for all crystals. The magnetic and structural transition at 134 K is clearly visible for the $BaFe_2As_2$ crystals and displays a similar shape to previous reports [4,14,29]. There is no significant variation in the temperature of the structural and magnetic transition with proton irradiation for any crystals, nor in the shape of the resistivity with temperature curves. Taken together, these imply that the fundamental electronic structure remains unperturbed by the damage. The most important observation, within the context of this study, is that the proton damage systematically increases the residual resistivity in both families of crystals, implying that only temperature-independent disorder has been added.

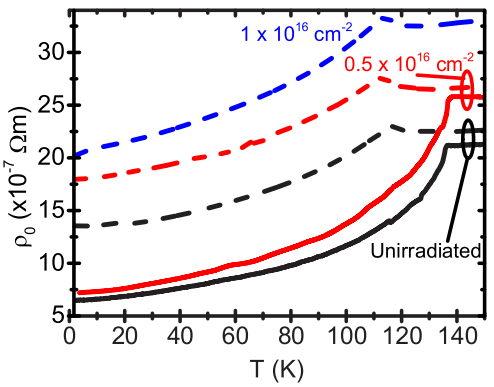

FIG. 1. (Color online) Zero-field resistivity (ρ_0) vs temperature for all samples. Solid lines, $BaFe_2As_2$; dashed lines, $BaFe_{1.985}Co_{0.015}As_2$.

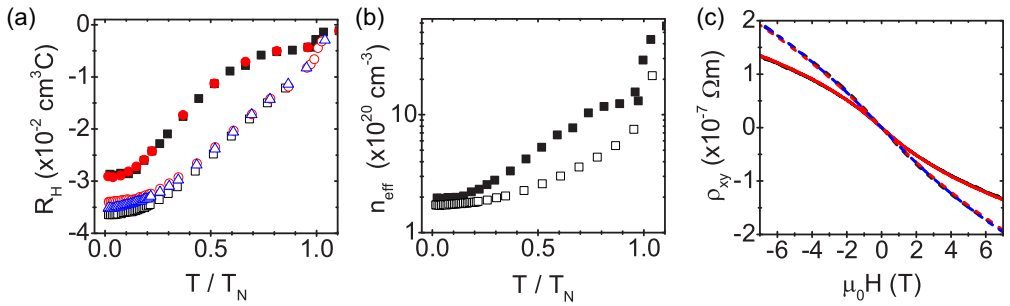

FIG. 2. (Color online) (a) Hall coefficient at 1 T vs temperature normalized by T_N for $BaFe_2As_2$ (solid symbols) and $BaFe_{1.985}Co_{0.015}As_2$ (open symbols). Unirradiated, ■□; 0.5×10^{16} cm^{-2}, ●○; 1×10^{16} cm^{-2}, △. (b) Effective carrier density (n_{eff}) against reduced temperature for unirradiated crystals. (c) Hall resistivity at 25 K for all $BaFe_2As_2$ (solid lines) and $BaFe_{1.985}Co_{0.015}As_2$ (dashed lines) samples. Black lines, unirradiated; red lines, 0.5×10^{16} cm^{-2}; blue line, 1×10^{16} cm^{-2}.

This observation is further supported by examining the low field Hall resistivity [$\rho_{xy}(\mu_0 H)$] data. For all crystals, a negative Hall coefficient indicative of electron carrier dominance is measured, as indicated in Fig. 2(a). The important observation is that the Hall coefficient is unaffected by the proton irradiation. This implies that the carrier density is unchanged by the proton damage, supporting the observation that the change in ρ_0 is primarily due to changes in scattering density and not changes in carrier concentration.

The temperature dependence of the Hall coefficient is quite different in the two compounds. We can compare behavior most simply by plotting the Hall coefficient against the temperature normalized by the magnetic transition temperature (T_N), as shown in Fig. 2(a). The difference between the curves suggests that Co doping significantly alters the electronic structure. Note that, as in other studies [30–32], we observe an increase in the magnitude of the Hall coefficient with Co doping. Within the Boltzmann transport model [see Eq. (6)], this signifies a decrease in carrier concentration rather than the expected increase in electron density with the addition of Co, as shown in Fig. 2(b). In Fig. 2(c), a direct comparison of $\rho_{xy}(\mu_0 H)$ at 25 K is shown for all crystals. The curves are nonlinear and more significantly so in the parent compounds. This curvature has been analyzed simply in terms of multicarrier behavior [15]. Due to the complexity of the electronic structure of these materials, no conclusive explanation has been generated to explain these trends.

We note that the insensitivity of the $\rho_{xy}(\mu_0 H)$ to changes in the scattering density (N_i) observed in this study is in contrast to that seen in the work conducted by Ishida *et al.* [15]. In that work, the magnetotransport properties were strongly influenced by annealing, leading to an eradication of the linear MR. This would suggest that extrinsic scatterers play a fundamental role in determining the magnetotransport properties. Furthermore, the study by Urata *et al.* [33] on Mn-doped $BaFe_2As_2$ observed that both the magnitude and shape of the $\rho_{xy}(\mu_0 H)$ was affected by the introduction of magnetic scatterers caused by Mn doping. Our work would suggest, however, that both annealing and Mn doping do not solely reduce/increase the number of scattering centers and therefore the exact nature of defects existent in the undoped and underdoped ferropnictides plays an essential role in determining the magnetotransport properties.

Let us now turn to the MR. We find that all crystals show a large linear component to the MR below the magnetic transition. Figures 3(a) and 3(b) show the characteristic field dependence for the symmetrized MR data for the unirradiated and 0.5×10^{16} cm^{-2} proton damaged $BaFe_2As_2$ crystals, respectively. In Fig. 3(c), the MR is compared at 10 K for both crystals. Figures 4(a), 4(b), and 4(c) show the characteristic field dependence for the symmetrized MR data for the unirradiated, 0.5×10^{16} and 1×10^{16} cm^{-2} proton damaged $BaFe_{1.985}Co_{0.015}As_2$ crystals respectively. In Fig. 4(d), the MR is compared at 10 K for all $BaFe_{1.985}Co_{0.015}As_2$ crystals. Both the temperature dependence and magnitude isare comparable to those of previous studies for both compounds [14,15]. The changes with irradiation are subtle.

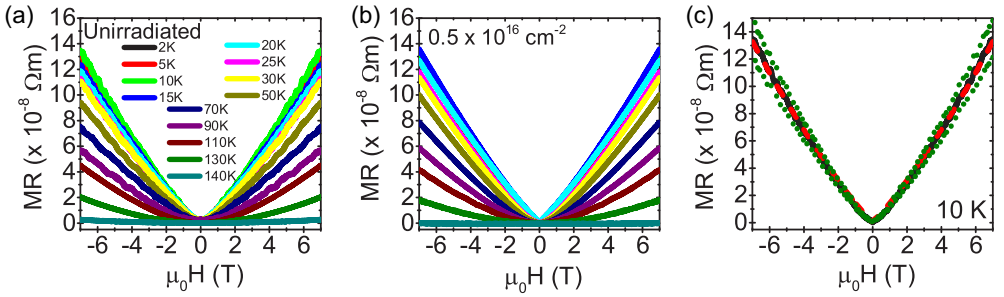

FIG. 3. (Color online) The field dependence of the symmetrized MR for unirradiated (a) and 0.5×10^{16} cm^{-2} irradiated (b) $BaFe_2As_2$ crystals. (c) Comparison between unirradiated (solid black line) and 0.5×10^{16} cm^{-2} irradiated (dashed red line) MR at 10 K for $BaFe_2As_2$ crystals. Green dotted lines represent ±10% change in MR.

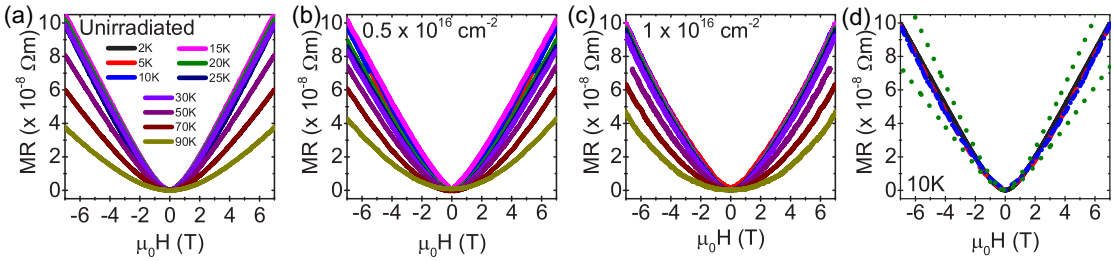

FIG. 4. (Color online) The field dependence of the symmetrized MR for unirradiated (a), 0.5×10^{16} cm^{-2} irradiated (b), and 1×10^{16} cm^{-2} (c) $BaFe_{1.985}Co_{0.015}As_2$ crystals. (d) Comparison between unirradiated (black solid line), 0.5×10^{16} cm^{-2} (red dashed line), and 1×10^{16} cm^{-2} (blue dash-dotted) irradiated MR at 10 K for $BaFe_{1.985}Co_{0.015}As_2$ crystals. Green dotted lines represent $\pm 25\%$ change in MR.

By taking the derivative of the symmetrized MR data, the functional form of the MR response can be observed. As shown in Fig. 5(a), the $BaFe_2As_2$ crystals show a linear contribution to the MR originating at fields above 1 T. The undoped crystals display a noticeable curvature at high fields, similar to earlier studies [14,34]. However, with Co doping the high field behavior of the unirradiated $BaFe_{1.985}Co_{0.015}As_2$ crystal shows increased linearity, reminiscent of the work of Kuo *et al.* [14]. However, with increasing irradiation the high field MR of the $BaFe_{1.985}Co_{0.015}As_2$ crystals becomes increasingly nonlinear, as shown in Fig. 5(b).

The B^* is extracted and plotted against reduced temperature in Figs. 5(c) and 5(d) for the $BaFe_2As_2$ and $BaFe_{1.985}Co_{0.015}As_2$ crystals, respectively. The expected T^2 relationship is coarsely perceived, as indicated by previous studies [8,35]. From this region, the Fermi velocity ($\sim 2 \times 10^5$ ms^{-1}) and energy (~ 3 meV) have been calculated using Eq. (3). These values correspond well with previous transport [8] and quantum oscillation work [36]. However, near T_N the data appear to deviate from this T^2 temperature dependence. Note that this deviation of B^* has been predicted theoretically [28].

Let us review our findings. From the in-plane and transverse resistivity we have established that the proton damage has changed the scattering density and in no other way changed the crystal properties. Figures 3(c) and 4(d) show that the changes to the MR as a result of the irradiation are subtle. We are now able to examine the influence of this increased scattering density on the high-field MR in comparison with the trends indicated by Eqs. (4) or (5) of the QLM model. To consider this we have fitted the high field MR above B^* using Eq. (3) and extracted the coefficients A_1 and O. A significant linear A_1 component exists for both the $BaFe_2As_2$ and the $BaFe_{1.985}Co_{0.015}As_2$ crystals, as shown in Figs. 6(a) and 6(d), respectively. Both the A_1 and the O coefficients in the $BaFe_2As_2$ crystals are insensitive to the increased scattering [see Figs. 6(a) and 6(b)].

It might be argued that the change in scattering density due to proton irradiation over the preexisting background defect scattering is small, and therefore changes in A_1 might be difficult to determine. Considering the change in the residual ρ_0 value as a rule of thumb guide to the change in scattering density, we estimate that the residual resistivity changes by 10% and 25% for 0.5×10^{16} cm^{-2} proton irradiation for the $BaFe_2As_2$ and $BaFe_{1.985}Co_{0.015}As_2$ crystals, respectively. In order to show whether changes of this order of magnitude are discernible, we include curves in Figs. 3(c) and 4(d) that show how a $\pm 10\%$ or $\pm 25\%$ change to the MR would manifest. We conclude that changes in the scattering density of this order of magnitude would be discernible if Eqs. (4) or (5) were applicable.

In $BaFe_{1.985}Co_{0.015}As_2$ the fitting procedure we have applied appears to show that the A_1 coefficient decreases by 30% at the highest irradiation commensurate with a significant increase in the quadratic component [see Figs. 6(d) and 6(e)], leaving the MR curve relatively unchanged [as shown in Fig. 4(d)]. We cannot rule out that this might be a feature of the fitting procedure rather than a physical change in the scattering properties of the various bands given that the overall change in the MR as a result of the irradiation are, in fact, rather subtle. A decrease of A_1 with increased N_i corresponds to the compensated QLM prediction expressed in Eq. (4). However, it is extremely unlikely that the ideal compensation within the DCs is achieved in the electron-doped $BaFe_{1.985}Co_{0.015}As_2$

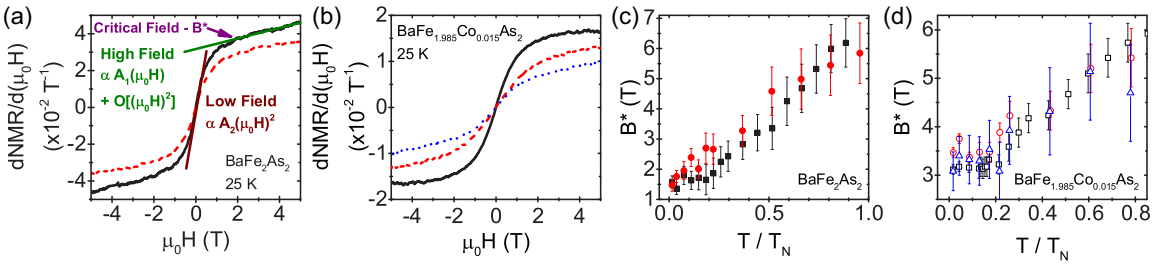

FIG. 5. (Color online) (a) NMR at 25 K for $BaFe_2As_2$ crystals; at low fields (dark red line) MR shows the conventional $(\mu_0 H)^2$ dependence; however, at high fields the MR has a significant linear component (green line). (b) NMR at 25 K for $BaFe_{1.985}Co_{0.015}As_2$ crystals. Black solid lines, unirradiated; red dashed lines, 0.5×10^{16} cm^{-2}; blue dotted line, 1×10^{16} cm^{-2}. (c) and (d) Critical field vs scaled temperature for $BaFe_2As_2$ (solid symbols) and $BaFe_{1.985}Co_{0.015}As_2$ crystals (open symbols), respectively. Unirradiated, ■□; 0.5×10^{16} cm^{-2}, ●○; 1×10^{16} cm^{-2}, △.

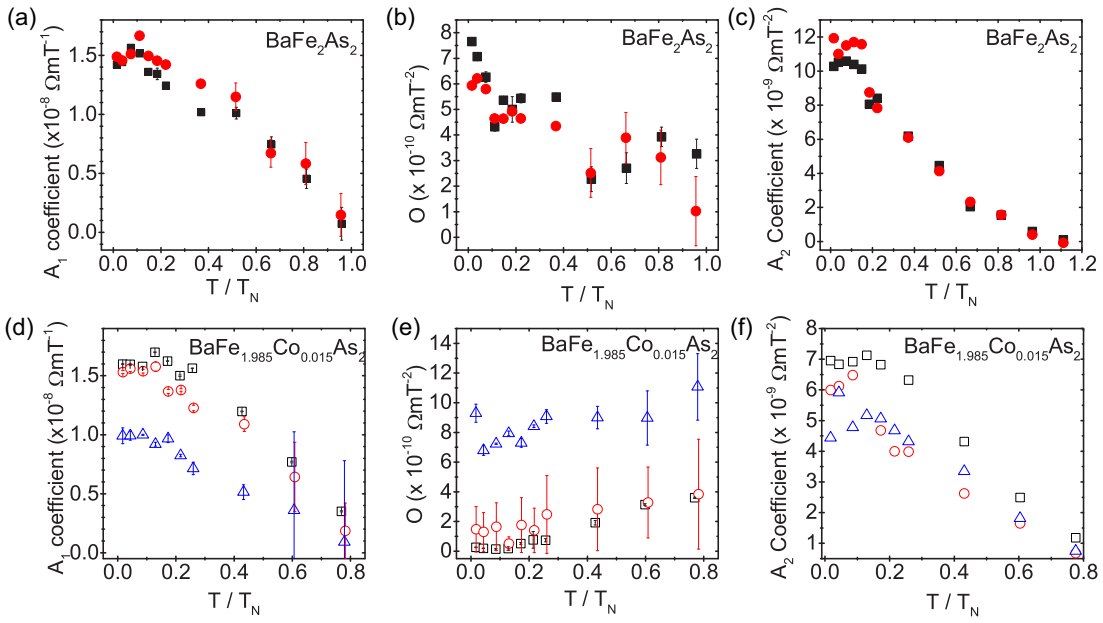

FIG. 6. (Color online) (a) and (d) A_1 coefficient for $BaFe_2As_2$ (solid symbols) and $BaFe_{1.985}Co_{0.015}As_2$ (open symbols) crystals respectively. (b) and (e) O coefficient for $BaFe_2As_2$ and $BaFe_{1.985}Co_{0.015}As_2$ crystals respectively. (c) and (f) A_2 coefficient for $BaFe_2As_2$ and $BaFe_{1.985}Co_{0.015}As_2$ crystals respectively. Unirradiated: ■□, 0.5×10^{16} cm^{-2}: ●○, 1×10^{16} cm^{-2}: △.

crystals. Clearly, the MR behavior in the $BaFe_{1.985}Co_{0.015}As_2$ crystals contravenes the QLM prediction as set out in Eqs. (4) and (5).

For completeness we also fit the low field parabolic behavior below B^* and this is parameterized using a coefficient A_2, which is shown in Figs. 6(c) and 6(f) for the undoped and Co-doped crystals, respectively. No systematic change in the A_2 coefficient is observed in either compound with irradiation.

In order to scrutinize the behavior of the undoped crystals in more detail, the temperature dependence of the A_1 coefficient is compared directly with the QLM predictions expressed in Eqs. (4) and (5), as shown in Fig. 7(a). To estimate N_i, it is necessary to derive the mean free path (mfp),

$$\text{mfp} = \frac{m^* v_F}{\rho_0 e^2 n} = \frac{m^* v_F \mu_H}{e} = \frac{E_F \mu_H}{e v_F}, \tag{7}$$

where m^* is the effective mass. The E_F and v_F values have been taken from the ARPES data from Richard *et al.* [10]. Using the mfp it is then possible to calculate N_i:

$$N_i = \frac{1}{\frac{4}{3}\left(\frac{\text{mfp}}{2}\right)^3}. \tag{8}$$

The 2 K N_i values are found to be 1.5×10^{26} m^{-3} for the unirradiated and 2.05×10^{26} m^{-3} for the irradiated parent crystals (suggesting a change in the scattering density due to 0.5×10^{16} cm^{-2} proton damaged of the order of 30%). The theoretical temperature dependencies of the compensated [Eq. (4)] and uncompensated [Eq. (5)], plotted using the derived 2K N_i values, clearly do not reflect the experimental A_1 temperature dependence.

Taken together, we can state with some certainty that the irradiation study shows that the linear MR is inconsistent with the QLM prediction for both undoped and Co-doped crystal families. As others have discussed in the context of applying the QLM to topological insulators [37], the necessary carrier density to satisfy the EQL is orders of magnitude too small. Using the experimental B^* value, the required density is $\sim 10^{17}$ cm^{-3}, whereas the experimentally derived carrier density is 2×10^{20} cm^{-3} for $BaFe_2As_2$ at 2 K. While the single carrier model that we have used to derive the carrier density may be subject to error, it is clear that, for any reasonable carrier concentration, achieving the EQL leads to an A_1 coefficient substantially larger than the experimental value.

B. Exploration of alternative models

Nonsaturating linear MR has been observed in a variety of materials, such as topological insulators [37–39], $SrTiO_3$ [40], cuprates [41–43], bismuth-based layered magnetic [44] and nonmagnetic [11] compounds, metal oxides [45], silver chalcogenides [46], graphene[47], and bismuth [48]. The QLM model appears to be good description for the final three materials, while the mechanism is less clear for the others. Recently, the balance equation proposal has been applied by Wang and Lei [49] to explain linear MR in the two-dimensional surface states of three-dimensional topological insulators. In its original form, the balance equation proposal is potentially applicable to the ferropnictides [50]. The proposal suggests that the high field MR magnitude should be proportional to the carrier density [49]. We have explored this by plotting the A_1 coefficient multiplied by n_{eff}^2 against n_{eff}. As shown in Figs. 7(b) and 7(c), discrepancies appear between the compounds. In the $BaFe_2As_2$ unirradiated crystal, a linear relationship is observed, which is not the case for the unirradiated $BaFe_{1.985}Co_{0.015}As_2$ crystal. However, the balance equation approach is predicted to be directly proportional to the effective magnetic g factor [49]. In the ferropnictides, the magnetic g factor is relatively small [51], suggesting this model is unlikely to be applicable.

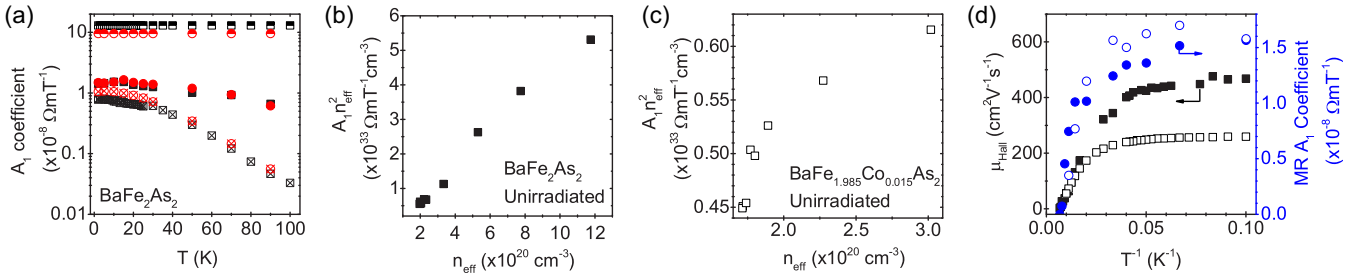

FIG. 7. (Color online) Experimental (■●), QLM compensated Eq. (4) (◓), and QLM uncompensated Eq. (5) (☒) A_1 coefficients for $BaFe_2As_2$ crystals for temperatures below 100 K. Black symbols, unirradiated; red symbols, 0.5×10^{16} cm^{-2}. A_1 coefficient multiplied by n_{eff}^2 vs n_{eff} for unirradiated (b) $BaFe_2As_2$ and (c) $BaFe_{1.985}Co_{0.015}As_2$ crystals. (d) μ_H and MR A_1 coefficient as a function of inverse temperature for unirradiated $BaFe_2As_2$ (■●) and $BaFe_{1.985}Co_{0.015}As_2$ (□○) crystals.

A recent paper by Koshelev [28] has explained the linear MR in terms of the FS reconstruction generated at the SDW magnetic transition. The SDW order leads to the mixing of the hole and electron bands and the creation of areas within the FS where the velocity of the carriers abruptly changes, so-called turning points. At these turning points, the normal orbital motion of the carriers in an applied magnetic field is disrupted, producing at low field an increased quadratic MR response and, above a crossover magnetic field, linear magnetoconductivity. Both the linear magnetoconductivity coefficient and B^* should depend on scattering within this model. B^* should vary proportionally with the inverse of the scattering time; i.e., B^* should increase with increased N_i. The extraction of B^* from our data is subject to significant uncertainty [see error bars shown in Figs. 5(c) and 5(d)] and within these limits it is difficult to determine the trends. However, we find that the difference in magnitude of B^* between the parent and the Co-doped crystals is consistent with this theory.

Further clues lie in the observation that we find a correspondence in the temperature evolution of μ_H and MR A_1 coefficient. As shown in Fig. 7(d), the temperature dependence for both parameters is shown to be consistent throughout the entire temperature range in both compounds. This finding echoes the work in the topological insulators [52], Heusler alloys [53], and MnAs-GaAs semiconductors [54], indicating that the linear MR may be proportional to the μ_H.

The nonlinearity and shape of $\rho_{xy}(\mu_0 H)$ in $BaFe_2As_2$ and $BaFe_{1.985}Co_{0.015}As_2$, as shown in Fig. 2(c), bears a similarity to that of the heavy fermion [55] and cuprate [41] superconductors. This nonlinearity is still not fully understood in any of these material families, although the anomalous Hall effect has been proposed as an explanation [56]. However, as has been pointed out by many authors, the ferropnictides, heavy fermion materials, and cuprates share a number of similar properties—AFM magnetic ground state, the two-dimensional nature of the electronic structure, and the existence of high-temperature superconductivity [57]—suggesting a common explanation [56] for the magnetotransport behavior.

To study the high field behavior of the Hall resistivity systematically, the high field (5–7 T) linear slope of the Hall resistivity has been calculated. An extremely surprising result emerges, as shown in Figs. 8(a) and 8(b). It appears that the intercept of high field Hall (HFH) resistivity linear fitting is independent of Co doping. Without a conclusive theoretical model for the origin of the $\rho_{xy}(\mu_0 H)$ nonlinearity, it is impossible to understand the significance of this observation. However, it would suggest that an intrinsic property of the magnetic state is retained despite Co doping.

It is useful if we now revisit the MR properties in light of the HFH effect observations. Due to the complexities of producing analytical models for the magnetotransport properties, scaling techniques are conventionally used. Kohler's rule is the traditionally used scaling method for understanding the temperature evolution of the MR ratio. When a single species of charge carrier exists such that $\frac{m^*}{ne^2}$ remains constant, then MR can be rescaled by dividing the applied magnetic field by the ρ_0:

$$\text{MR ratio}(\mu_0 H, T) = f\left[\frac{\mu_0 H}{\rho(0,T)}\right]. \tag{9}$$

In Fig. 8(c), the Kohler plots for 10 K, 25 K, 50 K, and 70 K are shown for the unirradiated $BaFe_{1.985}Co_{0.015}As_2$ crystal. As indicated by the failure of the lines to fall upon a single curve, Kohler's rule is clearly contravened. Furthermore, the refined Kohler rule [58], where the temperature dependence of the scattering is taken into account, does not illustrate any clear scaling. To explain violations of the Kohler rule, a modified form of Kohler scaling has been developed where the MR is scaled by the Hall angle ($\tan\theta_H = \frac{\rho_{xy}}{\rho_{xx}}$):

$$\text{MR ratio}(\mu_0 H, T) = f\left(\frac{\mu_0 H}{\tan^2\theta_H}\right). \tag{10}$$

This has been shown to more accurately scale both the cuprate [59] and the heavy fermion [60] superconductors. The compounds studied in this work display intriguing differences. For $BaFe_2As_2$, the modified Kohler form does not provide any improvement at any temperature below T_N, as indicated by the inset of Fig. 8(d). In contrast, the modified Kohler analysis illustrates a strong correlation at low temperatures for $BaFe_{1.985}Co_{0.015}As_2$. This pattern follows that of Ru doping indicated by Eom *et al.* [61]. It has been suggested that the modified Kohler rule could originate from an anisotropic scattering rate due to spin fluctuations [61]. In the anisotropic scattering rate scenario, the dominant electron-electron scattering process shows a large disparity within the FS due to the SDW magnetic order [62]. This produces locations of larger/smaller electron and hole scattering rates, leading to so-called hot/cold spots which dominate the magnetotransport

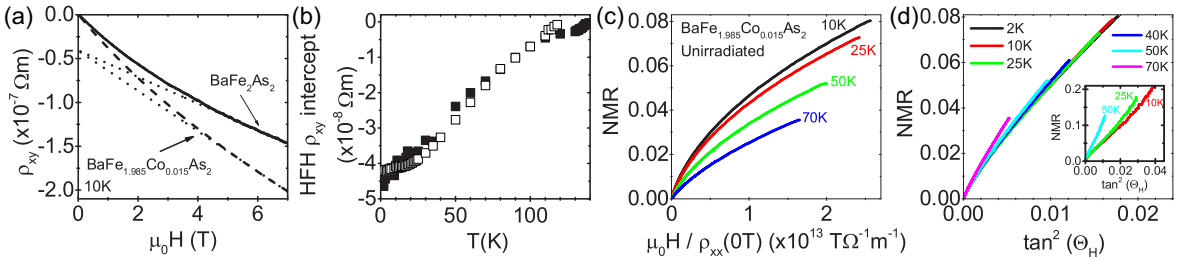

FIG. 8. (Color online) (a) Hall resistivity for unirradiated $BaFe_2As_2$ (solid line) and $BaFe_{1.985}Co_{0.015}As_2$ (dashed line) crystal at 10 K. Dotted lines are linear fits of high field Hall resistivity. (b) High field Hall resistivity intercept against temperature for unirradiated crystals. $BaFe_2As_2$, ■; $BaFe_{1.985}Co_{0.015}As_2$, □. (c) Kohler plots for unirradiated $BaFe_{1.985}Co_{0.015}As_2$ crystal. (d) Modified Kohler plots for unirradiated $BaFe_{1.985}Co_{0.015}As_2$ crystal. (Inset) Modified Kohler plots for unirradiated $BaFe_2As_2$ crystal.

properties. It is important to note that the anisotropic scattering model has been shown to recreate the unusual Hall coefficient dependence of Co doping discussed previously [62]. Nevertheless, the model would have to reconcile the differences we find between the undoped and Co-doped crystals, where the former shows similar nonlinear HFH but yet its MR does not scale according to the modified Kohler rule.

IV. CONCLUSION

In summary, using the systematic introduction of scattering centers through 3-MeV proton irradiation, we have studied the effect of defects on the normal-state magnetotransport properties of high-quality undoped $BaFe_2As_2$ and electron-doped $BaFe_{1.985}Co_{0.015}As_2$ single crystals. We have demonstrated that the proton damage increases the scattering density and does not strongly affect other properties. The high field MR exhibits a nonsaturating linear MR in all crystals, as seen in previous studies. However, we observe discrepancies between the compounds. In the undoped $BaFe_2As_2$ crystals, no change in the high field linear component is observed upon irradiation. In contrast, the $BaFe_{1.985}Co_{0.015}As_2$ crystals appear to display a decrease in the A_1 coefficient with proton irradiation, and an increasing quadratic component, although the changes to the MR curves with irradiation are, in fact, quite subtle. These observations are not consistent with the application of the QLM model in the ferropnictides. In addition, the Hall resistivity has been measured with increasing irradiation dose and displays a consistent nonlinearity at high fields and below 100 K for all crystals, irrespective of proton irradiation. Furthermore, the magnitude of the Hall coefficient is unaffected by the introduction of scattering defects. We have compared our observed trends with theoretical predictions. The multiband nature of the materials makes the magnetotransport trends complex and a simple explanation elusive. Nevertheless, setting out how these crystal families react to systematic increase in scattering density helps to lay the foundations for further theoretical developments.

ACKNOWLEDGMENTS

D.M. and A.S. acknowledge support from the US Department of Energy, Basic Energy Sciences, Materials Sciences and Engineering Division. L.F.C. and K.Y. acknowledge support from the UK funding agency the EPSRC Grant No. EP/H040048/1.

[1] Z. P. Yin, K. Haule, and G. Kotliar, Nat. Mater. **10**, 932 (2011).
[2] J. Paglione and R. Greene, Nat. Phys. **6**, 645 (2010).
[3] M. D. Johannes and I. I. Mazin, Phys. Rev. B **79**, 220510 (2009).
[4] A. S. Sefat, M. A. McGuire, R. Jin, B. C. Sales, D. Mandrus, F. Ronning, E. D. Bauer, and Y. Mozharivskyj, Phys. Rev. B **79**, 094508 (2009).
[5] M. Rotter, M. Tegel, D. Johrendt, I. Schellenberg, W. Hermes, and R. Pöttgen, Phys. Rev. B **78**, 020503 (2008).
[6] I. I. Mazin, M. D. Johannes, L. Boeri, K. Koepernik, and D. J. Singh, Phys. Rev. B **78**, 085104 (2008).
[7] P. Dai, J. Hu, and E. Dagotto, Nat. Phys. **8**, 709 (2012).
[8] K. K. Huynh, Y. Tanabe, and K. Tanigaki, Phys. Rev. Lett. **106**, 217004 (2011).
[9] T. Morinari, E. Kaneshita, and T. Tohyama, Phys. Rev. Lett. **105**, 037203 (2010).
[10] P. Richard, K. Nakayama, T. Sato, M. Neupane, Y.-M. Xu, J. H. Bowen, G. F. Chen, J. L. Luo, N. L. Wang, X. Dai, Z. Fang, H. Ding, and T. Takahashi, Phys. Rev. Lett. **104**, 137001 (2010).
[11] K. Wang, D. Graf, and C. Petrovic, Phys. Rev. B **87**, 235101 (2013).
[12] I. Pallecchi, F. Bernardini, M. Tropeano, A. Palenzona, A. Martinelli, C. Ferdeghini, M. Vignolo, S. Massidda, and M. Putti, Phys. Rev. B **84**, 134524 (2011).
[13] D. Bhoi, P. Mandal, P. Choudhury, S. Pandya, and V. Ganesan, Appl. Phys. Lett. **98**, 172105 (2011).
[14] H.-H. Kuo, J.-H. Chu, S. C. Riggs, L. Yu, P. L. McMahon, K. De Greve, Y. Yamamoto, J. G. Analytis, and I. R. Fisher, Phys. Rev. B **84**, 054540 (2011).
[15] S. Ishida, T. Liang, M. Nakajima, K. Kihou, C. H. Lee, A. Iyo, H. Eisaki, T. Kakeshita, T. Kida, M. Hagiwara, Y. Tomioka, T. Ito, and S. Uchida, Phys. Rev. B **84**, 184514 (2011).
[16] Y. Nakajima, T. Taen, Y. Tsuchiya, T. Tamegai, H. Kitamura, and T. Murakami, Phys. Rev. B **82**, 220504 (2010).

[17] N. Haberkorn, B. Maiorov, I. O. Usov, M. Weigand, W. Hirata, S. Miyasaka, S. Tajima, N. Chikumoto, K. Tanabe, and L. Civale, Phys. Rev. B **85**, 014522 (2012).
[18] M. P. Delmo, S. Yamamoto, S. Kasai, T. Ono, and K. Kobayashi, Nature (London) **457**, 1112 (2009).
[19] J. Fenton and A. J. Schofield, Phys. Rev. Lett. **95**, 247201 (2005).
[20] C. Herring, J. Appl. Phys. **31**, 1939 (1960).
[21] O. Entin-Wohlman, Y. Levinson, and A. G. Aronov, Phys. Rev. B **49**, 5165 (1994).
[22] F. J. Ohkawa, Phys. Rev. Lett. **64**, 2300 (1990).
[23] A. A. Abrikosov, Europhys. Lett. **49**, 789 (2000).
[24] A. A. Abrikosov, J. Phys. A: Math. Gen. **36**, 9119 (2003).
[25] Y. Tanabe, K. K. Huynh, S. Heguri, G. Mu, T. Urata, J. Xu, R. Nouchi, N. Mitoma, and K. Tanigaki, Phys. Rev. B **84**, 100508 (2011).
[26] A. S. Sefat, R. Jin, M. A. McGuire, B. C. Sales, D. J. Singh, and D. Mandrus, Phys. Rev. Lett. **101**, 117004 (2008).
[27] L. J. van der Pauw, Philips Res. Rep. **13**, 1 (1958).
[28] A. E. Koshelev, Phys. Rev. B **88**, 060412 (2013).
[29] A. S. Sefat, D. J. Singh, R. Jin, M. A. McGuire, B. C. Sales, F. Ronning, and D. Mandrus, Physica C (Amsterdam, Neth.) **469**, 350 (2009).
[30] E. D. Mun, S. L. Bud'ko, N. Ni, A. N. Thaler, and P. C. Canfield, Phys. Rev. B **80**, 054517 (2009).
[31] L. Fang, H. Luo, P. Cheng, Z. Wang, Y. Jia, G. Mu, B. Shen, I. I. Mazin, L. Shan, C. Ren, and H.-H. Wen, Phys. Rev. B **80**, 140508 (2009).
[32] F. Rullier-Albenque, D. Colson, A. Forget, and H. Alloul, Phys. Rev. Lett. **103**, 057001 (2009).
[33] T. Urata, Y. Tanabe, K. K. Huynh, H. Oguro, K. Watanabe, S. Heguri, and K. Tanigaki, Phys. Rev. B **89**, 024503 (2014).
[34] S. V. Chong, G. V. M. Williams, J. Kennedy, F. Fang, J. L. Tallon, and K. Kadowaki, Europhys. Lett. **104**, 17002 (2013).
[35] Y. Tanabe, K. K. Huynh, T. Urata, S. Heguri, G. Mu, J. T. Xu, R. Nouchi, and K. Tanigaki, Phys. Rev. B **86**, 094510 (2012).
[36] J. G. Analytis, C. M. J. Andrew, A. I. Coldea, A. McCollam, J.-H. Chu, R. D. McDonald, I. R. Fisher, and A. Carrington, Phys. Rev. Lett. **103**, 076401 (2009).
[37] S. X. Zhang, R. D. McDonald, A. Shekhter, Z. X. Bi, Y. Li, Q. X. Jia, and S. T. Picraux, Appl. Phys. Lett. **101**, 202403 (2012).
[38] H. Tang, D. Liang, R. Qiu, and X. Gao, ACS Nano **5**, 7510 (2011).
[39] B. A. Assaf, T. Cardinal, P. Wei, F. Katmis, J. S. Moodera, and D. Heiman, Appl. Phys. Lett. **102**, 012102 (2013).
[40] Z. Q. Liu, W. M. Lü, X. Wang, Z. Huang, A. Annadi, S. W. Zeng, T. Venkatesan, and Ariando, Phys. Rev. B **85**, 155114 (2012).
[41] G. Li and E. Y. Andrei, Nat. Phys. **3**, 623 (2007).
[42] M. van Zalk, A. Brinkman, and H. Hilgenkamp, J. Phys.: Condens. Matter **23**, 205602 (2011).
[43] P. M. C. Rourke, A. F. Bangura, C. Proust, J. Levallois, N. Doiron-Leyraud, D. LeBoeuf, L. Taillefer, S. Adachi, M. L. Sutherland, and N. E. Hussey, Phys. Rev. B **82**, 020514 (2010).
[44] K. Wang, D. Graf, L. Wang, H. Lei, S. W. Tozer, and C. Petrovic, Phys. Rev. B **85**, 041101 (2012).
[45] A. D. Rata, V. Kataev, D. Khomskii, and T. Hibma, Phys. Rev. B **68**, 220403 (2003).
[46] M. Lee, T. F. Rosenbaum, M. L. Saboungi, and H. S. Schnyders, Phys. Rev. Lett. **88**, 066602 (2002).
[47] A. L. Friedman, J. L. Tedesco, P. M. Campbell, J. C. Culbertson, E. Aifer, F. K. Perkins, R. L. Myers-Ward, J. K. Hite, C. R. Eddy, G. G. Jernigan, and D. K. Gaskill, Nano Lett. **10**, 3962 (2010).
[48] L. Li, J. G. Checkelsky, Y. S. Hor, C. Uher, A. F. Hebard, R. J. Cava, and N. P. Ong, Science (New York, NY) **321**, 547 (2008).
[49] C. M. Wang and X. L. Lei, Phys. Rev. B **86**, 035442 (2012).
[50] X. L. Lei and C. S. Ting, Phys. Rev. B **30**, 4809 (1984).
[51] J. J. Ying, T. Wu, Q. J. Zheng, Y. He, G. Wu, Q. J. Li, Y. J. Yan, Y. L. Xie, R. H. Liu, X. F. Wang, and X. H. Chen, Phys. Rev. B **81**, 052503 (2010).
[52] C. Shekhar, S. Ouardi, G. H. Fecher, A. Kumar Nayak, C. Felser, and E. Ikenaga, Appl. Phys. Lett. **100**, 252109 (2012).
[53] C. Shekhar, S. Ouardi, A. K. Nayak, G. H. Fecher, W. Schnelle, and C. Felser, Phys. Rev. B **86**, 155314 (2012).
[54] H. G. Johnson, S. P. Bennett, R. Barua, L. H. Lewis, and D. Heiman, Phys. Rev. B **82**, 085202 (2010).
[55] Y. Nakajima, H. Shishido, H. Nakai, T. Shibauchi, K. Behnia, K. Izawa, M. Hedo, Y. Uwatoko, T. Matsumoto, R. Settai, Y. Onuki, H. Kontani, and Y. Matsuda, J. Phys. Soc. Jpn. **76**, 024703 (2007).
[56] S. Nair, S. Wirth, S. Friedemann, and F. Steglich, Adv. Phys. **61**, 583 (2012).
[57] T. Shibauchi, A. Carrington, and Y. Matsuda, Annu. Rev. Condens. Matter Phys. **5**, 113 (2014).
[58] X. Ding, Y. Pan, H. Yang, and H.-H. Wen, Phys. Rev. B **89**, 224515 (2014).
[59] J. M. Harris, Y. F. Yan, P. Matl, N. P. Ong, P. W. Anderson, T. Kimura, and K. Kitazawa, Phys. Rev. Lett. **75**, 1391 (1995).
[60] D. Gnida, M. Matusiak, and D. Kaczorowski, Phys. Rev. B **85**, 060508 (2012).
[61] M. J. Eom, S. W. Na, C. Hoch, R. K. Kremer, and J. S. Kim, Phys. Rev. B **85**, 024536 (2012).
[62] A. F. Kemper, M. M. Korshunov, T. P. Devereaux, J. N. Fry, H.-P. Cheng, and P. J. Hirschfeld, Phys. Rev. B **83**, 184516 (2011).